Fuel 359 (2024) 130458

Contents lists available at ScienceDirect

Fuel

journal homepage: www.elsevier.com/locate/fuel

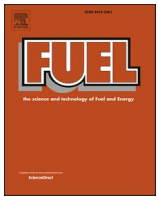

Short communication

Solventless autothermic production of energy-intensive furanic biofuels expedited by photothermal effect

Jinshu Huang [a], Jiasheng Chen [a], Zhuochun Huang [a], Tengyu Liu [a], Yan Ding [a], Hu Li [a,*], Chao He [b,*]

[a] National Key Laboratory of Green Pesticide, Key Laboratory of Green Pesticide & Agricultural Bioengineering, Ministry of Education, State-Local Joint Laboratory for Comprehensive Utilization of Biomass, Center for R&D of Fine Chemicals, Guizhou University, Guiyang, Guizhou 550025, China
[b] Faculty of Engineering and Natural Sciences, Tampere University, Korkeakoulunkatu 8, 33720 Tampere, Finland

ARTICLE INFO

Keywords:
Biomass conversion
Biofuels
Photothermal effect
Solvent-free reaction
Biomass-based materials

ABSTRACT

Driving C-C coupling reactions to produce biofuels is usually energy-consuming and requires well-tailored catalysts. Herein, a novel photothermal catalytic strategy was developed to be highly efficient for cascade hydroxyalkylation-alkylation (HAA) of various biomass-derived aldehydes/ketones with 2-methylfuran or acetalization of different bioalcohols with furfural to exclusively afford furanic biofuel molecules (up to 94.8 % yield). The developed bio-based SO_3H-functionalized graphene-like catalyst (GLB-SO_3H-700) could complete the HAA and acetalization reactions in 10 min under solvent-free and room-temperature conditions. Infrared thermal imaging revealed that the local photothermal effect of interfacial solar heating could *in-situ* remove water co-product, thereby improving the reaction selectivity and rate as evidenced by kinetic study. Moreover, the GLB-SO_3H-700 catalyst exhibited good stability and recyclability. The developed SO_3H-functionalized graphene-like photothermal materials hold great potential for catalytic upgrading of biomass into high-quality biofuels under mild conditions.

1. Introduction

Biomass is the fourth largest energy source after coal, oil, and natural gas, with annual output exceeding 140 billion metric tons (dry weight) in the world, which is 10 times larger than global energy consumption [1,2]. Compared with fossil fuels, the most obvious advantages of renewable biomass are wide distribution, large reserves, and low cost. At present, catalytic conversion of biomass into value-added chemicals and biofuels has been widely reported [3,4]. Among them, the obtained biomass derivatives like alkanes, furans, alcohols, and lipids are potential biofuels, while most of them are C5-C6 molecules, which cannot meet the carbon number (C9-C20) required for gasoline and diesel [5]. Therefore, it is highly promising to develop carbon-increasing strategies for energy-intensive biofuels.

In comparison with conventional C—C coupling catalytic processes, such as Aldol condensation, ketonization, Diels–Alder, Guerbet, and acylation reactions, the cascade reaction of hydroalkylation-alkylation (HAA) can more effectively increase the carbon-chain length of the platform molecules via the sequential double condensation process [5]. For example, biomass-derived 5-hydroxymethylfurfural (5-HMF), levulinic acid (LA), and furfural (FAL) could be subjected to HAA reaction with 2-methylfuran (2-MF) to prepare C8-C15 biofuels [6,7]. Both homogeneous (e.g., sulfuric acid, *p*-toluenesulfonic acid, phosphoric acid and trifluoromethanesulfonic acid) and heterogeneous (e.g., Pd/$NbOPO_4$, P-SiO_2, TFA-ZrO_2, Ir-ReO_x/SiO_2, $Si_{66}C_{33}$HT-SO_3H and Cu$(OTf)_2$) acid catalysts have been used to drive the HAA condensation reactions under relatively harsh conditions (up to 140 °C for 2–24 h, Scheme 1) [8–12]. The co-product during HAA to furnish the carbon-increased biofuels is water, which not only impedes the complete proceeding of the reaction but also interacts with the used catalysts and reactants to cause adverse effects (e.g., catalyst deactivation and side reactions) [13]. Given this, the key to the high-efficiency production of energy-intensive biofuels with specific carbon-chain length from biomass is to develop efficient protocols for in-situ removal of water from heterogeneous acid catalysts to break the reaction equilibrium with improved conversion/selectivity and maintain the intact structure of the catalyst.

Sunlight is a green, clean, and sustainable energy source, providing

* Corresponding authors.
E-mail addresses: hli13@gzu.edu.cn (H. Li), chao.he@tuni.fi (C. He).

https://doi.org/10.1016/j.fuel.2023.130458
Received 13 September 2023; Received in revised form 3 November 2023; Accepted 19 November 2023
Available online 23 November 2023

energy for all life activities on earth through emitting ultraviolet (UV), visible, and infrared (IR) lights that carry photons of different vibration frequencies [14]. Interestingly, interfacial solar heating and local photothermal effects with high solar utilization show great potential in the fields of seawater desalination, sewage treatment, and photothermal catalysis [15], with the assistance of various photothermal materials like metal nanoparticles (e.g., Ag, Pd, Al, Cu, Ge, and Co), semiconductors (e.g., TiO_2, MoO_{3-x}, WO_{3-x}, ZnO, and CdO), carbon-based nanomaterials (e.g., carbon quantum dots, graphite, carbon nanotubes, and graphene), organic polymers (polythiophene, polypyrrole, polyaniline, and polydopamine), and two-dimensional transition metal carbides/nitrides [16]. In recent years, carbon-based nanomaterials have become a research hotspot in the field of photothermal catalysis due to their advantages of low cost, simple preparation method, stable chemical properties, broadband light absorption, high thermal conductivity, and adjustable molecular and electronic structures [16]. However, rare studies have been conducted on the catalytic production of energy-intensive biofuels via photothermally driven HAA or other relevant reactions of renewable biomass feedstocks under mild conditions.

Here, a biomass-derived SO_3H-functionalized graphene-like catalyst (GLB-SO_3H-700) was facilely prepared from *Chlorella* residue after lipid extraction, combining the tunable acidity of carbon-based nanomaterials with the local photothermal effect of solar heating. Under sunlight irradiation, the prepared functional material could rapidly form a high local temperature in the reaction system, which is beneficial to the removal of *in-situ* produced water. In addition, the generated high local temperature has another two obvious advantages: (i) It would be favorable for the formation of temperature difference in the reaction system, which is conducive to the transfer of non-radiative relaxation of excited electrons to the material lattice and the realization of efficient light conversion into heat energy; (ii) It can benefit the diffusion of reactants and the desorption of products, accelerating the overall reaction rate. With the renewed carbon-increasing strategy via cascade HAA enabled by the tunable photothermal effect, this study realizes the high-efficiency catalytic conversion of biomass derivatives into energy-intensive furanic biofuel molecules in specifically increased carbon numbers at room temperature within a quite short reaction time of 10 min (Scheme 1).

2. Experimental

SO_3H-functionalized graphene-like catalyst (GLB-SO_3H-700) was prepared from *Chlorella* residue after lipid extraction [17] by sequential calcination and sulfonation with H_2SO_4, according to previous literature [18,19] with slight modifications. The catalyst structure and properties were investigated by infrared thermal imaging, Raman, XRD, XPS, SEM, TEM, NH_3-TPD, and thermogravimetric analysis.

For a detailed list of chemicals and reagents, see Supplementary Material Text S1. The specific preparation procedures and methods of GLB-T and GLB-SO_3H-T photothermal catalysts are shown in Supplementary Material (Text S2.1 & S2.2). Catalyst characterization is described in detail in Supplementary Material (Text S2.3). The detailed procedures and analysis methods for the synthesis of furanic biofuel molecules by HAA or acetalization are provided in Supplementary Material (Text S2.4). The reusability of the catalyst and the acid density analysis method and procedures are supplied in Supplementary Material (Text S2.5 & S2.6).

3. Results and discussion

3.1. Catalyst characterization

In the HAA reaction process, acidic catalysts are usually indispensable and water is formed as the dominant co-product. Therefore, both the acidity and hydrophobicity of the developed photothermal materials (GLB-SO_3H-*T*, *T* denotes calcination temperature of 500, 700, and 900 °C) should be considered. FT-IR spectra of GLB-SO_3H-*T* illustrated that the characteristic peaks of -SO_3H appeared at 1021 cm^{-1} and 1258 cm^{-1} [20], which belonged to the symmetric and asymmetric stretching vibration of O═S═O, respectively, indicating the successful introduction of -SO_3H into the graphene-like structure (Fig. 1a). The full survey and C 1s XPS spectra revealed the presence of S element in the GLB-SO_3H-*T* catalysts and the formation of C—S bonds (Fig. 1b & S1) [21], which further confirmed the above FT-IR results. The water contact angle of GLB-SO_3H-700 was determined to be 139.1° (Fig. S2), suggesting its good hydrophobicity, which was conducive to the *in-situ* elimination of water generated in the HAA reaction.

To evaluate the performance of the photothermal material in the conversion of sunlight into heat energy, infrared thermal imaging was used to monitor the local temperature of the GLB-SO_3H-*T* (*T* = 500, 700, and 900 °C) catalysts (Fig. 1c). It was found that the temperature of the catalyst surface reached 54.5–78.7 °C after 2 min of light irradiation at 1000 W m^{-2}, which would be helpful to drive the HAA reaction. The involved mechanism of light conversion into heat over a photothermal catalyst was that the carbon-based material absorbs light and excites loose π electrons in the ground state to the excited state (Fig. S3), followed by transferring to the lattice of the carbon material through non-radiative relaxation in the form of excited phonons and vibrating to generate heat [20]. Therefore, the more ordered the lattice periodicity of the prepared catalyst was, the better the local photothermal effect could be observed. Furthermore, the periodicity of the material lattice also affected the transfer of heat, where the ordered lattice structure was more apt to facilitate the rapid transfer of heat to the reactant molecules, with great potential to improve the reaction selectivity and rate [22,23]. Raman spectra of GLB-SO_3H-*T* (*T* = 500, 700, and 900 °C) exhibited two broad characteristic peaks at 1345 cm^{-1} and 1645 cm^{-1} (Fig. S4), which

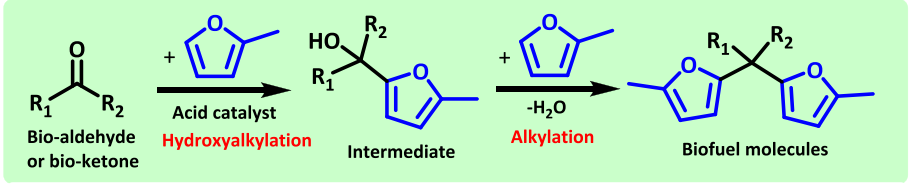

Previous work:
^ Long reaction time: 2-24 h
^ High reaction temperature: 50-140 °C
^ Driving force energy source: Heat
^ Co-product water inhibits the reaction
^ Homogeneous/heterogeneous acid catalyst

This work:
^ Short reaction time: 10 min
^ Low temperature: 25 °C
^ Driving force energy source: Light
^ *In-situ* water removal enables reaction
^ Bio-based photothermal catalyst

Scheme 1. Comparison of conventional methods and the developed photothermal catalytic protocol for producing energy-intensive furanic biofuels via cascade hydroalkylation-alkylation (HAA).

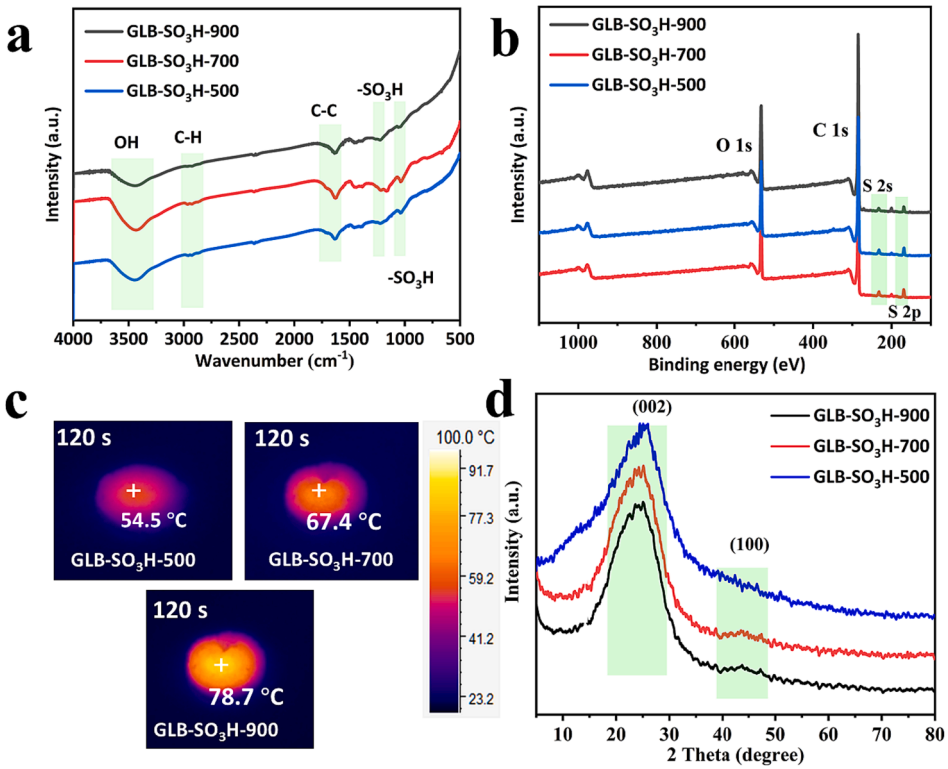

Fig. 1. FT-IR spectra (a), XPS spectra (b), infrared thermal images (c), and XRD patterns (d) of photothermal catalysts GLB-SO_3H-*T* (*T* = 500, 700, and 900 °C).

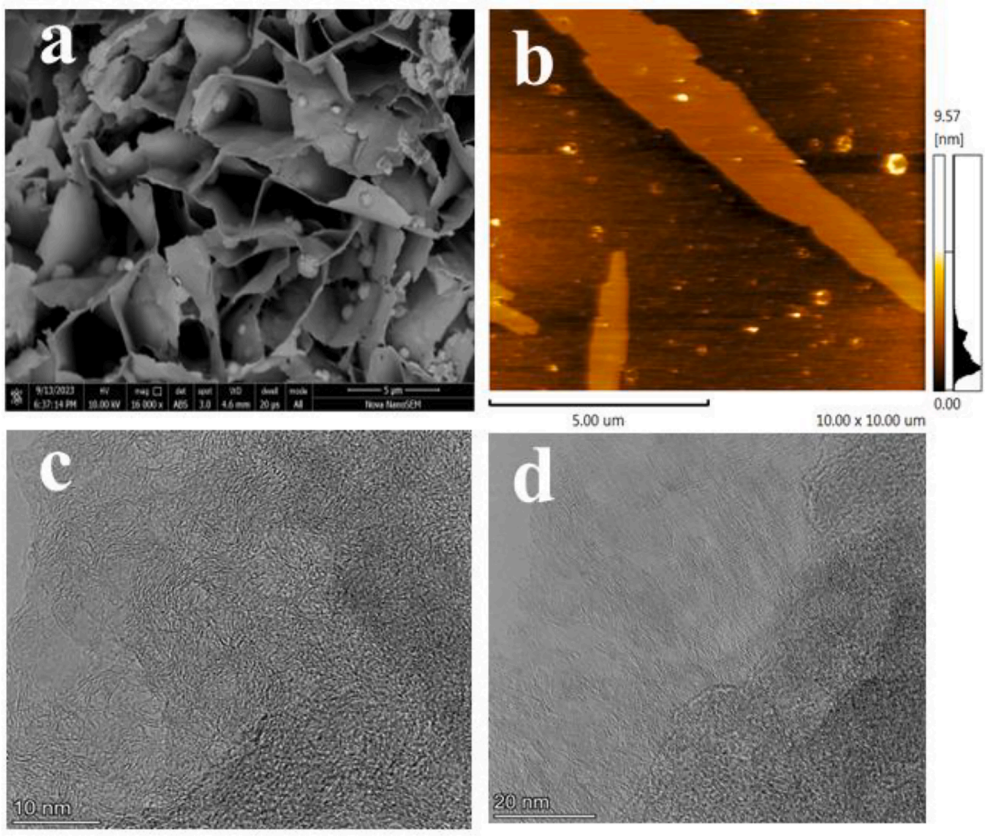

Fig. 2. SEM (a), AFM (b), and TEM (c,d) images of GLB-SO_3H-700.

could be attributed to the unique D and G bands of the carbon-based materials [24]. The I_D/I_G values of GLB-SO_3H-500, GLB-SO_3H-700, and GLB-SO_3H-900, negatively correlated with the degree of graphitization, were calculated to be 3.42, 3.18, and 3.02, respectively, which explicitly showed the tendency of the increasingly ordered lattice structure of the material with the increase of calcination temperature. XRD characterization (Fig. 1d) further clarified the crystal structure of the catalyst, and the diffraction peaks at 2θ of 23.2° and 44.1° demonstrated the existence of amorphous carbon with (0 0 2) crystalline plane and the graphite carbon structure with (1 0 0) facet, respectively [25,26]. The results of Raman, XRD, and infrared thermal imaging were mutually corroborated and congruously demonstrated that the higher the catalyst carbonization temperature was, the higher the catalyst graphitization degree and the better the photothermal effect would be observed. SEM and AFM images (Fig. 2a & 2b) revealed that GLB-SO_3H-700 was an irregularly stacked nanosheet structure. The irregularly stacked carbon layers and ripples could be clearly observed by TEM (Fig. 2c & 2d), which was consistent with the structure detected by SEM. The BET curve of GLB-SO_3H-700 was IV-type hysteresis, revealing that the catalyst was mesoporous (8.3 nm) with a relatively large specific surface area (234.2 m^2/g), which could be attributed to the irregularly stacked carbon layer structure of GLB-SO_3H-700 catalyst. It was worth noting that the carbon layer structure of GLB-SO_3H-700 would be conducive to providing more -SO_3H branching sites and larger reaction sites (Fig S5) [27–30].

The catalyst acidity was tested by NH_3-TPD (Figs. S6). Broad NH_3 desorption bands at 80.6 °C and 188.7 °C manifested the presence of weak and strong acid sites, respectively. In addition, it could also be found that the acidity of GLB-700 was significantly enhanced after sulfonation, which further clarified that the carbon catalyst was successfully sulfonated to afford GLB-SO_3H-700. The -SO_3H densities of GLB-SO_3H-500, GLB-SO_3H-700, and GLB-SO_3H-900 catalysts were measured by the Boehm titration method and found to be 2.89 mmol g^{-1}, 2.14 mmol g^{-1} and 1.21 mmol g^{-1}, respectively. The percentages of S atoms in these catalysts obtained by elemental analysis were 9.28, 6.85, and 3.88 % (Table S1), respectively, which were consistent with the results of the Boehm titration method. Notably, the catalyst density of -SO_3H was likely in agreement with its I_D/I_G value, which could be explained by the fact that the greater the degree of carbon disorder of the catalyst was, the more favorable the -SO_3H species could be introduced [31]. On the contrary, the catalyst (GLB-SO_3H-900) with a more ordered carbon lattice was not conducive to the introduction of -SO_3H.

The thermal stability of the GLB-SO_3H-700 catalyst was examined by thermogravimetric analysis (TGA) (Fig. S7). It was found that the weight loss of GLB-SO_3H-700 was ca. 8 % at 50–600 °C, which belonged to the volatilization and pyrolysis of H_2O and -SO_3H in the catalyst. The photothermal effect temperature of the system in this study could reach up to around 80 °C, which was much lower than the pyrolysis temperature of -SO_3H (ca. 200 °C). Therefore, the thermal stability of GLB-SO_3H-700 met the requirements of this reaction system.

3.2. Catalytic performance and mechanism

In preliminary studies, biomass-derived 2-MF and FAL in a molar ratio of 2:1 were selected as model molecules for HAA at room temperature (25 °C) over different catalysts including GLB-SO_3H-500, GLB-SO_3H-700, GLB-SO_3H-900, GLB-700 and H_2SO_4, and the obtained results are collected in Fig. 3a. Among the tested catalysts, GLB-SO_3H-700 catalyst was found to have the best catalytic performance in the production of 5,5′-(furan-2-ylmethylene)bis(2-methylfuran) (FMBM) (94.8 % yield) (Fig. S8) while a quite inferior yield (ca. 50.2 %) was obtained under otherwise identical but thermal conditions (~60 °C, Fig. 3a), implying that the photothermal effect and -SO_3H density of GLB-SO_3H-700 were both ideal for catalyzing the HAA reaction of FAL and 2-MF. In contrast, the GLB-SO_3H-500 with slightly worse lattice periodicity exhibited a relatively lower photothermal effect, while GLB-SO_3H-900 with a better periodicity of the lattice structure was unfavorable for the introduction of -SO_3H, resulting in a decrease in its acidity. Encouraged by its pronounced performance, the GLB-SO_3H-700 catalyst was further used to catalyze the HAA of various biomass-derived aldehydes/ketones with 2-MF or acetalization of bio-based alcohols with FAL, and high yields (77.4–94.8 %) of relevant furanic biofuel molecules could be obtained at 25 °C in 10 min, demonstrating the universal applicability of GLB-SO_3H-700 catalyst (Fig. 4).

For the ability of the GLB-SO_3H-700 catalyst to *in-situ* remove water, the local photothermal effect of interfacial solar heating was revealed by infrared thermal imaging (Fig. 1c), and the hydrophobic surface was disclosed by contact angle test (139.1°) (Fig. S2). In addition, the chemical equilibrium study was carried out for the photothermal catalyst GLB-SO_3H-700, and a comparison was made with the H_2SO_4-mediated catalytic system that could not generate the photothermal effect under otherwise identical conditions (Figs. S9 and S10). It could be found that the equilibrium conversion rate catalyzed by H_2SO_4 did not change with the rise of temperature, possibly because water generated in a homogeneous system could not be removed by evaporation, making the reaction reach a dynamic equilibrium quickly. In contrast, the equilibrium conversion rate catalyzed by the GLB-SO_3H-700 photothermal catalyst increased with the rise of photothermic temperature, indicating that the local photothermal system of GLB-SO_3H-700 was able to break the dynamic equilibrium and make the reaction move toward the positive direction, which might be due to continuous evaporation of generated water around acid sites. Overall, in the traditional H_2SO_4 catalytic system driven by electric heating, the yield of FMBM was maintained at 12.6–26.3 %. For the GLB-SO_3H-700 photothermally

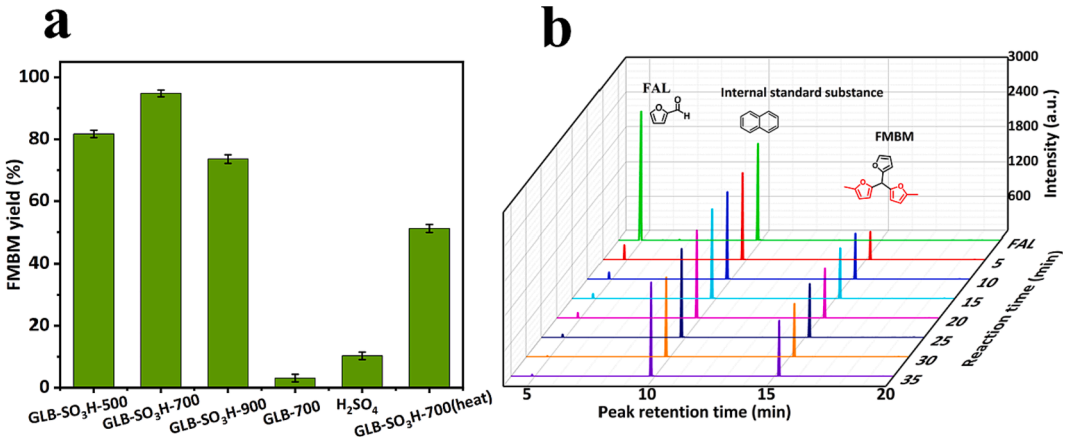

Fig. 3. The HAA reaction of 2-MF and FAL over different catalysts (4.3 mol%) at 25 °C in 10 min (a), and GC spectra of reaction mixtures after different times (b).

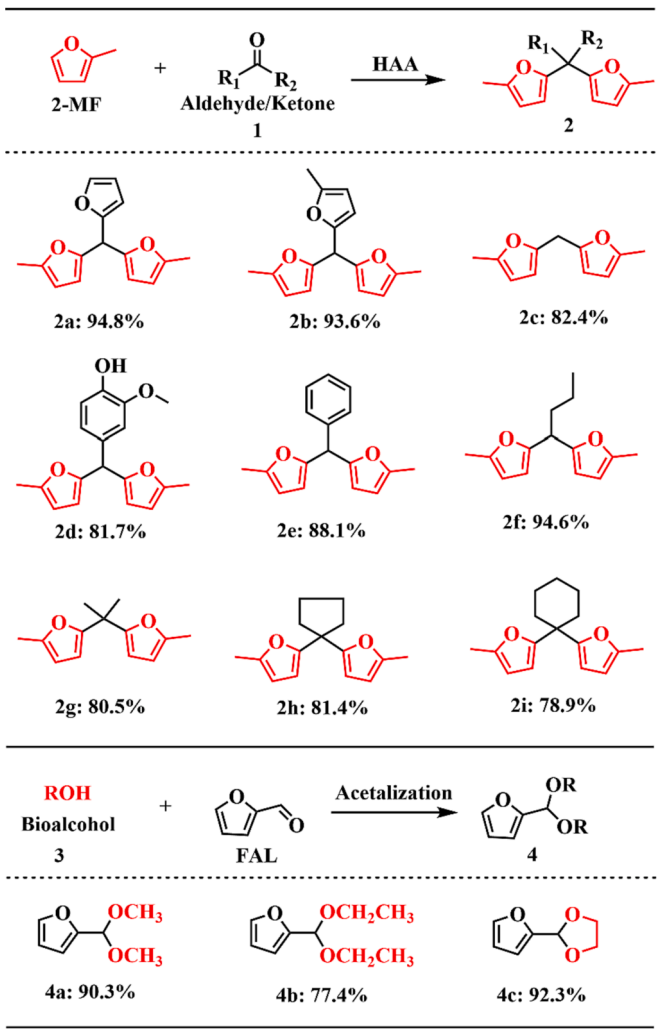

Fig. 4. Catalytic HAA of various bio-derived aldehydes/ketones with 2-MF or acetalization of bio-derived alcohols with FAL over GLB-SO_3H-700 to produce carbon-increasing furanic biofuel molecules. Reaction conditions: 4.3 mol% H^+ of GLB-SO_3H-700, 4 mmol 2-MF or bio-derived alcohols, 2 mmol bio-derived aldehyde/ketone or FAL, light intensity of 1000 W m^{-2}, 25 °C and time of 10 min.

driven catalytic system, the yield of FMBM increased with the increase of light intensity (25.5–74.4 %), further indicating that water in the reaction system could be effectively *in-situ* removed (Fig. S9).

Table 1 collects catalytic results of representative traditional thermal catalysts and the developed GLB-SO_3H-700 photothermal catalyst for the HAA of FAL and 2-MF to produce the biofuel molecule FMBM. With comparable and even superior activity to the previously reported catalysts, GLB-SO_3H-700 could accomplish the cascade conversion process in a much shorter reaction time (10 min) at a lower reaction temperature (25 °C). It was further expounded that the local high-temperature environment could be rapidly generated over the GLB-SO_3H-700 catalyst under light irradiation, and a temperature difference around its surroundings was formed in the reaction system, which could accelerate the diffusion of reactants and the desorption of products to reduce the occurrence of side reactions [32,33]. More importantly, the local high temperature was beneficial to remove water generated by the HAA reaction (step 2: alkylation), thus improving both the reaction rate and selectivity. No intermediates were detected by gas chromatography (GC) (Fig. 3b), which was attributed to the rapid dehydration of the generated dimer (bis(5-methylfuran-2-yl)methanol) (step 2), indicating that the reaction rate of step 2 (alkylation) was higher than that of step 1 (hydroxyalkylation). Moreover, our developed catalyst GLB-SO_3H-700 was found to exhibit superior activity to those carbon-based acid catalysts (Entries 3, 4, and 9, Table 1) under either thermal or photothermal conditions. It was further indicated that the high local temperature in the photothermal catalyst was beneficial to improve the reaction selectivity and eliminate the negative influence of water on the catalyst and reaction process.

3.3. Study of reaction kinetics and catalyst recyclability

Further, the involved reaction kinetics was studied and found to follow first-order kinetics (Fig. 5a & 5b) under different light intensities (500, 600, and 700 W m^{-2}) and reaction times (4, 6, 8, 10, and 12 min). The reaction activation energy of the developed photothermal system calculated by the Arrhenius formula and fitting formula (Fig. 5c) was 32.2 kJ mol^{-1}, which seemed not easy to take place at room temperature, indicating that the photothermal effect generated on the GLB-SO_3H-700 catalyst was crucial for its pronounced catalytic activity in HAA.

The reusability of heterogeneous catalysts is an important parameter to evaluate their stability. After five consecutive recycles of the GLB-SO_3H-700 catalyst, the obtained yield of FMBM was slightly reduced from 94.8 % to 90.6 % (Fig. 5d). The FT-IR and S 2p XPS spectra of the recovered and fresh GLB-SO_3H-700 catalysts (Figs. S11 & S12) showed the intact structure before and after the reaction. The good recyclability of GLB-SO_3H-700 should benefit from the rapid removal of co-product water enabled by the local photothermal system, effectively preventing the active -SO_3H group from hydrolysis/leaching. In addition, the rapid desorption of the formed product from the catalytically active

Table 1
Results of catalytic HAA of 2-MF and FAL using different catalysts.

Entry	Catalyst	Time	2-MF: FAL(n/n)	Temp. (°C)	Energy Source	FMBM yield (%)	Ref.
1	p-TSA	12 h	2.2:1	65	Heat	90	[24]
2	H_2SO_4	12 h	2.2:1	65	Heat	71.5	[24]
3	Commercial GO	6 h (10 min)	22:1	60	Heat (Light)	0 (0)[b]	[24]
4	S-MWCNTs	7 h (10 min)	2:1	85	Heat (Light)	90 (8.2)[b]	[34]
5	Amberlyst-15	24 h	2.2:1	50	Heat	95	[35]
6	Zr-SBA-15(20)	15 h	2.5:1	140	Heat	93.9	[36]
7	*p*-TOSH	2 h	2.3:1	70	Heat	78.4	[37]
8	Nafion-212	2 h	2:1	65	Heat	75	[38]
9	IGO	6 h (10 min)	22:1	60	Heat (Light)	95 (12.3)[b]	[24]
10	GLB-SO_3H-700	2 h (10 min)	2:1	60 (25[a])	Heat (Light)	96.2 (94.8)[b]	This work

[a] Initial reaction temperature.
[b] Light irradiation results.

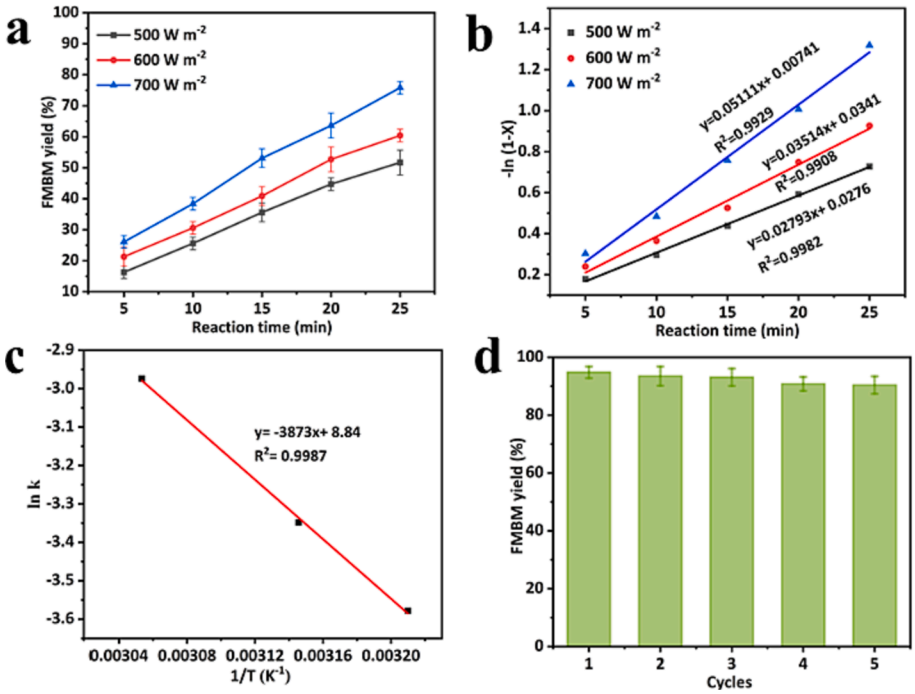

Fig. 5. Effect of light irradiation intensity and reaction time on FMBM yield (a). The linear relationship between -ln(1-*X*) and reaction time *t* (b). Linear fitting diagram of ln*k* and 1/*T* (c). Reusability study of GLB-SO_3H-700 (d).

surface might also contribute to the almost constant performance of GLB-SO_3H-700. Overall, the developed GLB-SO_3H-700 photothermal catalyst was greatly promising for conversion of biomass derivatives to produce high-quality furanic biofuels in specific carbon-chain lengths via cascade HHA and other relevant routes.

4. Conclusions

A photothermal material GLB-SO_3H-700 derived from *Chlorella* residue was developed to be efficient for the catalytic synthesis of high-quality furanic biofuel molecules under ambient conditions. Due to the local photothermal effect of solar interface heating, a high FMBM yield of up to 94.8 % was obtained through the efficient and solvent-free HAA carbon-increasing process at 25 °C within 10 min. In the GLB-SO_3H-700 mediated local photothermal system, the adverse effect of water on the reaction and catalyst was substantially eliminated to significantly improve the HAA reaction selectivity and rate. HAA of various biomass-derived aldehydes/ketones with 2-MF or acetalization of different bioalcohols with FAL to produce corresponding furanic biofuels could also be achieved using the developed catalytic system. In addition, GLB-SO_3H-700 with an appropriate -SO_3H density of 2.14 mmol g^{-1} and lattice structure in good periodicity exhibited excellent reusability after at least five cycles.

CRediT authorship contribution statement

Jinshu Huang: Writing – original draft, Validation, Methodology, Investigation. **Jiasheng Chen:** Formal analysis. **Zhuochun Huang:** Investigation. **Tengyu Liu:** Investigation. **Yan Ding:** Software. **Hu Li:** . **Chao He:** .

Declaration of competing interest

The authors declare that they have no known competing financial interests or personal relationships that could have appeared to influence the work reported in this paper.

Data availability

Data will be made available on request.

Acknowledgements

The authors thank financial support from the Guizhou Provincial S&T Project (GCC[2023]011, ZK[2022]011), National Natural Science Foundation of China (22368014), and Guizhou Provincial Higher Education Institution Program (Qianjiaoji[2023]082).

Appendix A. Supplementary material

Supplementary data to this article can be found online at https://doi.org/10.1016/j.fuel.2023.130458.

References

[1] Gao M, Zhang T, Ho GW. Advances of photothermal chemistry in photocatalysis, thermocatalysis, and synergetic photothermocatalysis for solar-to-fuel generation. Nano Res 2022;15:9985–10005.
[2] Kumari N, Chhabra T, Kumar S, Krishnan V. Nanoarchitectonics of sulfonated biochar from pine needles as catalyst for conversion of biomass derived chemicals to value added products. Catal Commun 2022;168:106467.
[3] Wang BY, Li M, Zhang S, Wu H, Liao Y, Li H. Synergistic effect between Co single atoms and nanoparticles enables selective synthesis of bio-based benzimidazoles. Appl Catal B-Environ 2023;327:122454.
[4] Meng Y, Jian Y, Li J, Wu H, Zhang H, Saravanamurugan S, et al. Surface-active site engineering: Synergy of photo-and supermolecular catalysis in hydrogen transfer enables biomass upgrading and H_2 evolution. Chem Eng J 2023;452:139477.
[5] Li H, Riisager A, Saravanamurugan S, Pandey A, Sangwan RS, Yang S, et al. Carbon-increasing catalytic strategies for upgrading biomass into energy-intensive fuels and chemicals. ACS Catal 2018;8:148–87.
[6] Konwar LJ, Samikannu A, Mäki-Arvela P, Mikkola J-P. Efficient C-C coupling of bio-based furanics and carbonyl compounds to liquid hydrocarbon precursors over lignosulfonate derived acidic carbocatalysts. Catal Sci Technol 2018;8:2449–59.
[7] Wang W, Li N, Li S, Li G, Chen F, Sheng X, et al. Synthesis of renewable diesel with 2-methylfuran and angelica lactone derived from carbohydrates. Green Chem 2016;18:1218–23.
[8] Liu S, Josephson TR, Athaley A, Chen QP, Norton A, Ierapetritou M, et al. Renewable lubricants with tailored molecular architecture. Sci Adv 2019;5: eaav5487.

[9] Andini E, Bragger J, Sadula S, Vlachos DG. Production of neo acids from biomass-derived monomers. Green Chem 2023;25:3493–502.
[10] Samikannu A, Konwar LJ, Rajendran K, Lee CC, Shchukarev A, Virtanen P, et al. Highly dispersed NbOPO4/SBA-15 as a versatile acid catalyst upon production of renewable jet-fuel from bio-based furanics via hydroxyalkylation-alkylation (HAA) and hydrodeoxygenation (HDO) reactions. Appl Catal B-Environ 2020;272:118987.
[11] Chhabra T, Dwivedi P, Krishnan V. Acid functionalized hydrochar as heterogeneous catalysts for solventless synthesis of biofuel precursors. Green Chem 2022;24:898–910.
[12] Ebikade EO, Sadula S, Liu S, Vlachos DG. Lignin monomer conversion into biolubricant base oils. Green Chem 2021;23:10090–100.
[13] Li H, Saravanamurugan S, Yang S, Riisager A. Catalytic alkylation of 2-methylfuran with formalin using supported acidic ionic liquids. ACS Sustain Chem Eng 2015;3:3274–80.
[14] Zhang X, Xue S-S, Pan W, Wang H, Wang K, Li N, et al. A heat shock protein-inhibiting molecular photothermal agent for mild-temperature photothermal therapy. Chem Commun 2023;59:235–8.
[15] Mateo D, Cerrillo JL, Durini S, Gascon J. Fundamentals and applications of photothermal catalysis. Chem Soc Rev 2021;50:2173–210.
[16] Cui X, Ruan Q, Zhuo X, Xia X, Hu J, Fu R, et al. Photothermal nanomaterials: A powerful light-to-heat converter. Chem Rev 2023;123:6891–952.
[17] Huang J, Wang J, Huang Z, Liu T, Li H. Photothermal technique-enabled ambient production of microalgae biodiesel: Mechanism and life cycle assessment. Bioresour Technol 2023;369:128390.
[18] Lu S-Y, Jin M, Zhang Y, Niu Y-B, Gao J-C, Li CM. Chemically exfoliating biomass into a graphene-like porous active carbon with rational pore structure, good conductivity, and large surface area for high-performance supercapacitors. Adv Energy Mater 2018;8:1702545.
[19] Kong X, Zhu Y, Lei H, Wang C, Zhao Y, Huo E, et al. Synthesis of graphene-like carbon from biomass pyrolysis and its applications. Chem Eng J 2020;399:125808.
[20] Huang J, Jian Y, Li H, Fang Z. Lignin-derived layered 3D biochar with controllable acidity for enhanced catalytic upgrading of Jatropha oil to biodiesel. Catal Today 2022;404:35–48.
[21] Luo J, Zhang C, Yao C, Ma D, Chen Y, Tian M, et al. Sulfur-doped activated carbon supported platinum species as robust catalysts for nitrobenzene hydrogenation to p-Aminophenol. Mol Catal 2023;545:113216.
[22] Wen G, Gu Q, Liu Y, Schlögl R, Wang C, Tian Z, et al. Biomass-derived graphene-like carbon: Efficient metal-free carbocatalysts for epoxidation. Angew Chem Int Ed 2018;57:16898–902.
[23] Wang R, Xia G, Zhong W, Chen L, Chen L, Wang Y, et al. Direct transformation of lignin into fluorescence-switchable graphene quantum dots and their application in ultrasensitive profiling of a physiological oxidant. Green Chem 2019;21:3343–52.
[24] Dutta S, Bohre A, Zheng W, Jenness GR, Núñez M, Saha B, et al. Solventless C-C coupling of low carbon furanics to high carbon fuel precursors using an improved graphene oxide carbocatalyst. ACS Catal 2017;7:3905–15.
[25] Gao J, Wang H, Cao X, Li Z, Guo H, Yang X, et al. Nitrogen doped carbon solid acid for improving its catalytic transformation of xylose and agricultural biomass residues to furfural. Mol Catal 2023;535:112890.
[26] Balotin G, De Almeida J, da Silva RM, Carvalho WA, Carvalho CT, Rodrigues R. Upgrading catalytic efficiency of activated carbons by tailoring lignocellulosic biomass waste for sustainable conversion of glycerol to solketal. Mol Catal 2023;538:112976.
[27] Wei X, Li W, Liu Q, Sun W, Liu S, Li S, et al. Pore-scale investigation on multiphase reactive transport for the conversion of levulinic acid to γ-valerolactone with Ru/C catalyst. Chem Eng J 2022;427:130917.
[28] Yang X, Wang J, Wei Y, Li B, Yan W, Yin L, et al. Cotton-derived carbon fiber-supported Ni nanoparticles as nanoislands to anchor single-atom Pt for efficient catalytic reduction of 4-nitrophenol. Appl Catal A-Gen 2022;643:118734.
[29] Choudhary P, Bahuguna A, Kumar A, Dhankhar SS, Nagaraja CM, Krishnan V. Oxidized graphitic carbon nitride as a sustainable metal-free catalyst for hydrogen transfer reactions under mild conditions. Green Chem 2020;22:5084–95.
[30] Shao Y, Sun K, Fan M, Wang J, Gao G, Zhang L, et al. Selective conversion of levulinic acid to gamma-valerolactone over Ni-based catalysts: Impacts of catalyst formulation on sintering of nickel. Chem Eng Sci 2022;248:117258.
[31] Zhang X, Navarathna CM, Leng W, Karunaratne T, Thirumalai RVKG, Kim Y, et al. Lignin-based few-layered graphene-encapsulated iron nanoparticles for water remediation. Chem Eng J 2021;417:129199.
[32] Song C, Wang Z, Yin Z, Xiao D, Ma D. Principles and applications of photothermal catalysis. Chem Catal 2022;2:52–83.
[33] Chhabra T, Dhingra S, Nagaraja CM, Krishnan V. Influence of Lewis and Brønsted acidic sites on graphitic carbon nitride catalyst for aqueous phase conversion of biomass derived monosaccharides to 5-hydroxymethylfurfural. Carbon 2021;183:984–98.
[34] Thombal PR, Thombal RS, Han SS. Comprehensive study on the catalytic methods for furyl alkane synthesis: A promising biodiesel precursor. Renew Sust Energ Rev 2021;135:110218.
[35] Zhong R, Liao Y, Peng L, Iacobescu RI, Pontikes Y, Shu R, et al. Silica–carbon nanocomposite acid catalyst with large mesopore interconnectivity by vapor-phase assisted hydrothermal treatment. ACS Sustain Chem Eng 2018;6:7859–70.
[36] Luo Y-J, Zhou Y-H, Huang Y-B. A new Lewis acidic Zr catalyst for the synthesis of furanic diesel precursor from biomass derived furfural and 2-methylfuran. Catal Lett 2019;149:292–302.
[37] Gebresillase MN, Shavi R, Seo JG. A comprehensive investigation of the condensation of furanic platform molecules to C14–C15 fuel precursors over sulfonic acid functionalized silica supports. Green Chem 2018;20:5133.
[38] Li G-G, Li N, Wang Z, Li C, Wang A, Wang X, et al. Synthesis of high-quality diesel with furfural and 2-methylfuran from hemicellulose. ChemSusChem 2012;5:1958–66.